Materials Today Communications 38 (2024) 108260

Contents lists available at ScienceDirect

Materials Today Communications

journal homepage: www.elsevier.com/locate/mtcomm

Modelling of coating thickness distribution on the edges of a moving cathode during electrogalvanizing

L.N. Bengoa [a,c,1], S.M. Goñi [b,c], V.O. Salvadori [b,c], P.R. Seré [a], P. Pary [a,c,*], W.A. Egli [a]

[a] Centro de Investigación y Desarrollo en Tecnología de Pinturas-CIDEPINT (CICPBA-CONICET-UNLP), Av. 52 121 y 122 s/n, 1900 La Plata, Argentina
[b] Centro de Investigación y Desarrollo en Criotecnología de Alimentos (CONICET-UNLP-CICPBA), 47 esq. 116, 1900 La Plata, Argentina
[c] Facultad de Ingeniería (UNLP), 1 y 47, 1900 La Plata, Argentina

ARTICLE INFO

Keywords:
Electrodeposition
Zinc
Simulation
Current distribution

ABSTRACT

Electrogalvanizing is a widespread practice used to prevent steel corrosion. A mathematical model was developed to simulate the plating process and to predict the zinc coating thickness distribution at the cathode surface for different operating conditions. The model considers ternary current distribution, diffusion and electric field migration in the solution, and electrodeposition of zinc on a moving steel cathode. Experiments were carried out to validate the model using an experimental device which reproduces the fluid dynamic and electrochemical conditions of the edges of a steel strip in an industrial electroplating line, the rotating washer electrode. The model was solved using the finite element software COMSOLTM Multiphysics. The developed model accurately predicts the average thickness obtained by gravimetric tests. The shapes of predicted deposits are in good agreement with the experimental ones. Consequently, the model provides a valuable tool to simulate different working conditions at the laboratory and promises to be quite useful to optimize industrial electroplating systems.

1. Introduction

Zinc electrodeposition on steel is a widespread practice used to prevent its corrosion. This protective coating system takes advantage of the more negative standard reversible potential of Zn towards that of Fe [1]. This makes zinc act as a sacrifice anode, preventing Fe oxidation. Continuous plating of zinc on steel sheet must produce a coating of uniform thickness with smooth appearance to accomplish strict surface quality constrains and, in the case of appliances and automotive panels [2] a good finish after painting is also needed.

Under specific conditions, zinc coating can be thicker at some singular points of the cathode, for example the edges of the strip and eventually, the growth of localized zinc deposits, *dendrites*, may occur as the steel strip passes through the different electrolytic cells. These fragile and loosely adhered material easily detach from the substrate during cutting and levelling processes, and some of them are dragged on the surface of the sheet. Then, in the press stamping or the bending processes, the zinc particles are imprinted in the surface of the material, causing a quality reject.

In the past, several fundamental investigations have elucidated the mechanism of dendrite growth during electrodeposition in stagnant electrolytes [3–7], and lately, Bengoa et al. developed an experimental device, the rotating washing electrode (RWE), that reproduce the hydrodynamic conditions and current distribution of the edges of the steel strip [8–11] with good experimental results regarding zinc coating distribution on the edge of the cathode and also with dendrite generation. In this work, the authors give the theoretical basis to the RWE, through process modeling and simulation tools to deeply understand how experimental conditions affect the coating thickness distribution on the edge of the moving cathode. Different modeling strategies have been proposed to simulate and optimize the electroplating process [12,13], in particular COMSOL Multiphysics software with the electrodeposition module allows the modeling of complex geometries. Among others, Robinson and Free [14] have modeled copper electrodeposition using cells of different geometries (a Hull cell and other with four cathodes); the authors presented an empirical equation to predict deposit thickness, by fitting COMSOL results. Werner et al. [15] demonstrated the ability of

* Corresponding author at: Centro de Investigación y Desarrollo en Tecnología de Pinturas-CIDEPINT (CICPBA-CONICET-UNLP), Av. 52 121 y 122 s/n, 1900 La Plata, Argentina.
E-mail address: p.pary@cidepint.ing.unlp.edu.ar (P. Pary).
[1] Present address: Novel Energy-Oriented Materials Group, Catalan Institute of Nanoscience and Nanotechnology ICN2 (CSIC-BIST), Edifici ICN2, Campus UAB, 08193 Bellaterra (Barcelona), Spain

https://doi.org/10.1016/j.mtcomm.2024.108260
Received 22 November 2023; Received in revised form 19 January 2024; Accepted 28 January 2024
Available online 1 February 2024

Nomenclature

A	Cathode surface area, m^2.
AT	Average thickness of zinc deposit, μm.
c	Concentration of chemical species, mole/m^3.
C_0	Oxidized species concentration, dimensionless, Eq. (6).
C_R	Reduced species concentration, dimensionless, Eq. (6).
D	Diffusion coefficient, m^2/s.
DOF	Degrees of freedom.
F	Faraday constant, 96485.34 Coulomb/mole.
I	Current, A.
i_0	Exchange current density, A/m^2.
i_C	Average current density, A/m^2.
$i_{C,local}$	Local current density, A/m^2.
p	Pressure, Pa.
r	Local radius, m.
R	Reaction velocity.
R_g	Universal gas constant.
t	Time, s.
T	Temperature, K.
U	Velocity field (vector, components u_r, u_w, u_z), m/s.
u_m	Mobility, s mol/kg.
z_c	Charge of chemical species, + 2 for Zn.
M	Mass, kg.
W	Rotation speed, rpm.

Subscripts

I	Initial.
F	Final.

Greeks letters

ρ	Fluid density, kg/m^3.
μ_T	Fluid turbulent viscosity, Pa*s.
μ	Fluid viscosity, Pa*s.
Φ_I	Potential in the electrolyte, V.
α_a	Anodic charge transfer coefficient.
α_c	Cathodic charge transfer coefficient.
η	Overpotential, V.

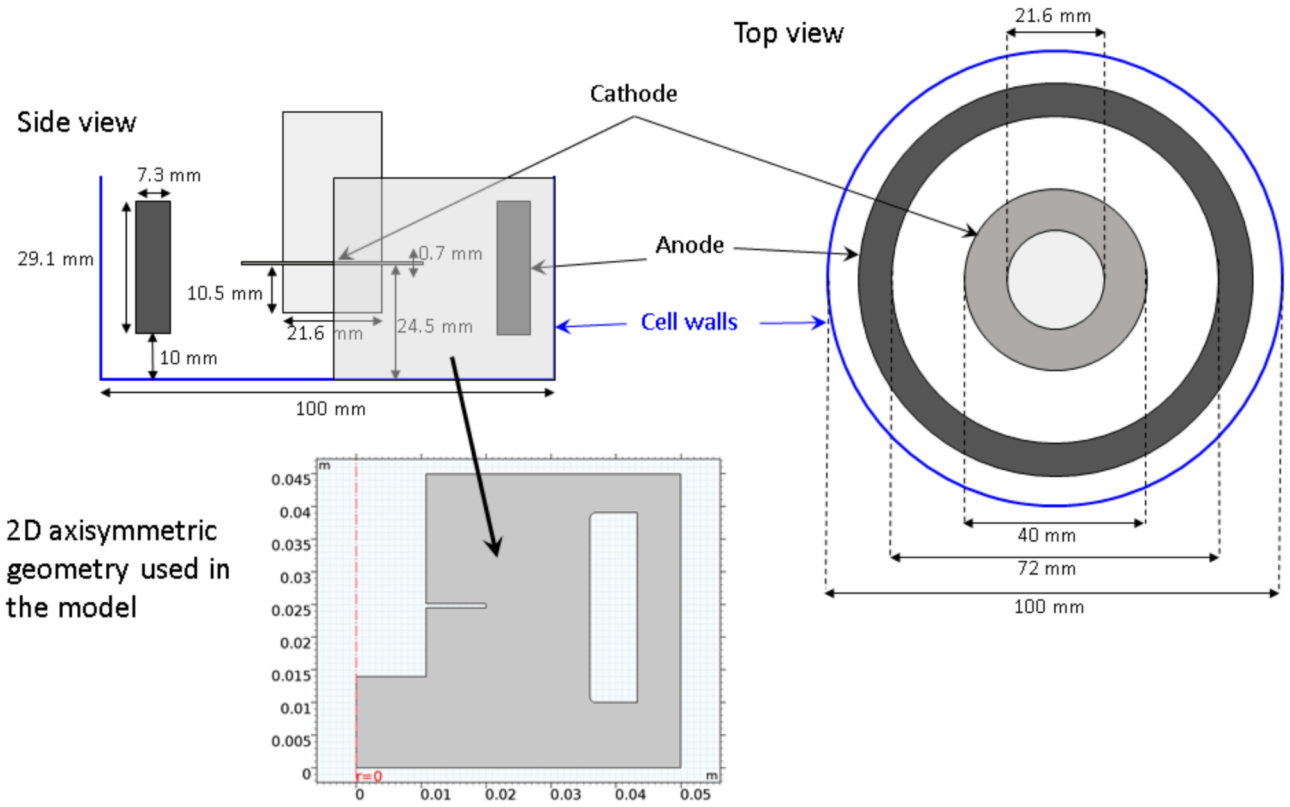

Fig. 1. Side and top representation of the system, and 2D axisymmetric geometric domain used in the mathematical model.

COMSOL Multiphysics 5.2a to simulate a copper electrowinning test cell. Mahapatro and Suggu [16] developed a mathematical model to investigate the effect of process parameters, i. e. current density and electrolyte conductivity, on copper electroplating. Da Cunha Bastos [17] analyzed the importance of spatial distribution of chemical species associated with the zinc-iron couple, in the corrosion protection of steel. The experimental cell was modeled using ternary current distribution, Nernst-Plank Interface, and different geometries and meshes were tested. Mohammed [18] developed an electrodeposition computer model involving mass transfer and electrode reactions, to simulate industrial plating operations. The model was validated with data from a Hull cell and from a custom build laboratory plating cell.

The aim of this work is to develop a useful tool to understand the fundamentals of the RWE and to predict the Zn thickness along the cathode. For that purpose, a mathematical model was proposed and solved using the software COMSOL™ Multiphysics. Finally, electrodeposition experiments on a RWE were carried out to contrast the data predicted by the model.

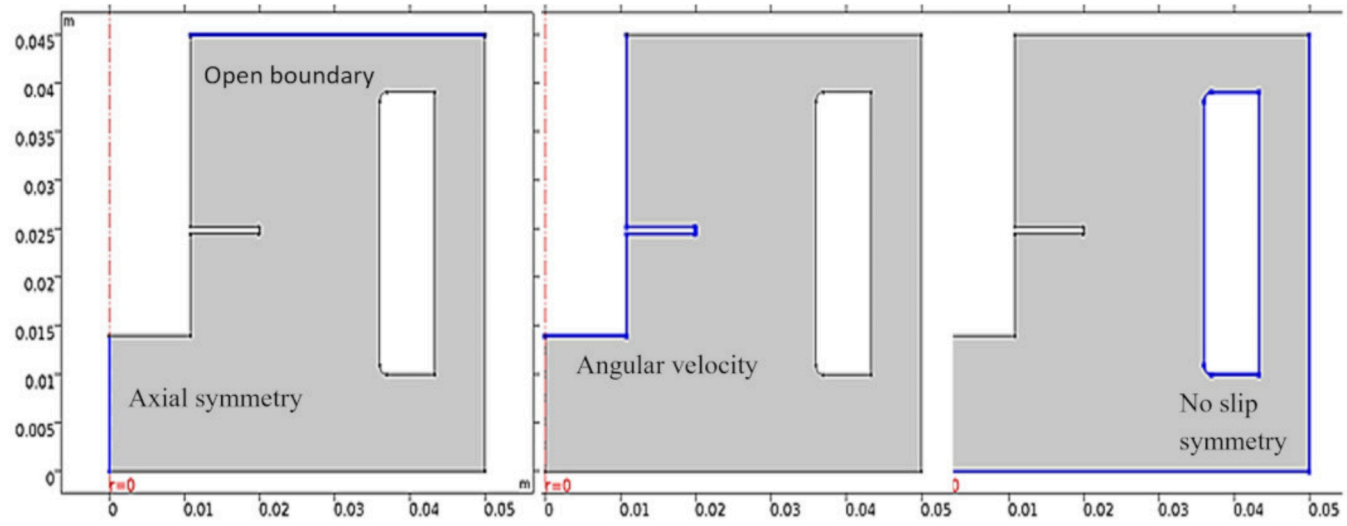

Fig. 2. Boundary conditions for momentum equations.

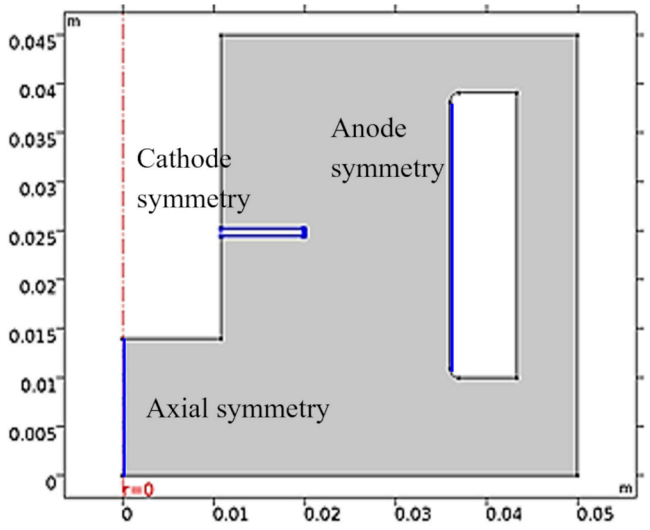

Fig. 3. Boundary conditions for ternary current distribution.

2. Materials and methods

2.1. Model description

A mathematical model was developed to simulate the plating process and to predict the zinc coating thickness distribution on the cathode surface for different operating conditions. Given the geometric features of the RWE available in our lab, a 2D axisymmetric domain was employed, which is composed of three domains (Fig. 1). The rotating axis and the cathode are located at the center of a cylindrical jar containing the electrolyte, whilst the static anode is in the outer section of the jar. Detailed sizes and locations of objects can be seen on Fig. 1.

The main transport phenomena considered in the experimental set up are:

- flow of the liquid contained in the jar due to rotating movement of the central rod and the cathode.
- ternary current distribution, with dissolution of Zinc in the anode, ions transport (convection, diffusion, and electric field migration) in the liquid solution, and electrodeposition of zinc in the cathode.

The described model was implemented in the finite element software COMSOL Multiphysics 5.3a (COMSOL AB, Sweden). Three modules available in the software were employed together: the fluid flow, the Nernst-Plank ternary current distribution, and deformed geometry interfaces. Next a summary of main governing equations is provided.

2.1.1. Fluid flow

In order to predict the fluid flow, the momentum (Navier-Stokes) and continuity equations (Eqs. (1) and (2)) were solved for incompressible flow, considering different turbulence models: the k-ε, k-ω and Shear Stress Transport (SST) turbulence models were tested [19,20].

$$\rho\frac{\partial u}{\partial t}+\rho(u\bullet\nabla)u=\nabla\bullet\left(-pI+(\mu+\mu_T)\left(\nabla u+(\nabla u)^T\right)\right) \quad (1)$$

$$\rho\nabla\bullet(u)=0 \quad (2)$$

where turbulent viscosity μ_T depends upon the turbulence model employed.

Boundary conditions for momentum equations were set as (Fig. 2):

- Axial symmetry in the fluid at $r = 0$.
- Open boundary at the top surface of the fluid.
- Prescribed angular velocity at the surface of rotating rod and cathode.
- No slip (zero velocity) in the walls of the device and anode.

In the numerical model, an average density of 1210 kg/m^3 was used, and a temperature dependent viscosity was adopted [21]. In preliminary studies the following strategies were tested:

- Simultaneous solution of fully coupled transient phenomena: fluid flow, ternary current distribution (see next section) and deposit formation.
- Sequential strategy:

o Step 1: simulation of the steady fluid flow.
o Step 2: simulation of the transient ternary current distribution coupled with deposit formation, using the velocity field of the steady fluid flow as a model input.

From the different turbulence models tested, SST was selected since it provides the best prediction of the fluid velocity near the rotating disk.

For both strategies the solver accounts for zinc deposit formation; the predicted deposit thicknesses along the cathode are very similar (differences in AT lower than 0.03%, result not shown); main differences

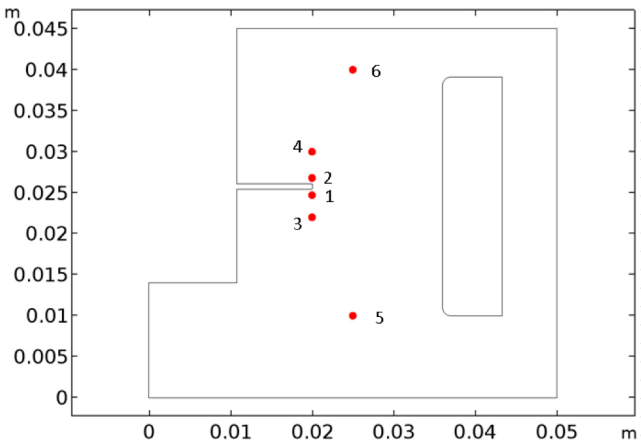

Fig. 4. Selected locations for the comparison of velocity.

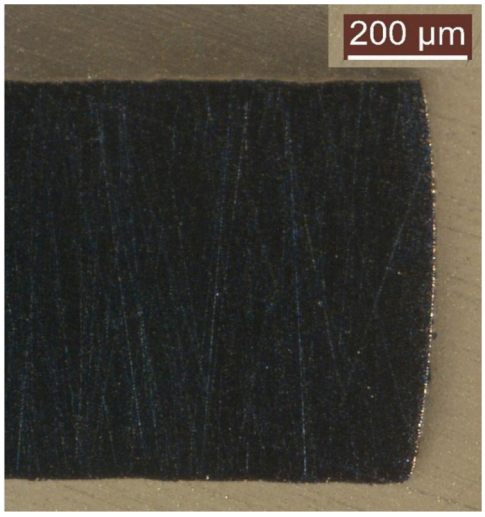

Fig. 5. Curved initial profile of the RWE obtained by optical microscopy.

Table 1
Experimental conditions for electrodeposition of Zn on the RWE.

Sample	i_C (A/dm^2)	Time (s)	*W* (rpm)	Temperature (°C)
1, 2, 3, 4	13.0	240	800	50
5	24.7	120	800	60
6	12.4	240	800	60
7	6.2	480	800	60
8	12.4	240	1200	60
9	12.4	240	400	60
10	12.4	240	800	50

arise in the fact that fully coupled solver increases the computational cost and simulation time. Consequently, the second strategy was employed to obtain the results presented in this work.

2.1.2. Ternary current distribution

The Nernst-Planck equation (Eq. (3)) with electro-neutrality was used to describe the ternary current distribution of Zn ions [15,22]:

$$\frac{\partial c}{\partial t} + \nabla \bullet (-D\nabla c - z_c u_m F c \nabla \phi_l + uc) = R \tag{3}$$

In the second term of Eq. (3), the three transport mechanisms are presented: diffusion, migration, and convection.

Boundary conditions for ternary current distribution (Fig. 3) were set as:

- Axial symmetry at $r = 0$
- In the cathode, the total current density i_C was set (Eq. (4)) according to experimental values, and a modified form of Butler–Volmer expression (a concentration dependent kinetics [15]) models the electrode kinetics (Eq. (5)).
- In the anode the electric potential was defined as V = 0, and similarly a concentration dependent kinetics was employed (Eq. (5)).
- In the remaining surfaces of the system, a no current flow boundary condition was imposed.

$$i_C = \frac{I}{A} \tag{4}$$

$$i_{C,local} = i_0\left(C_R \exp\left(\frac{\alpha_a F\eta}{RT}\right) - C_0 \exp\left(\frac{-\alpha_c F\eta}{RT}\right)\right) \tag{5}$$

2.1.3. Meshing and solver configuration

The simulation domain was discretised using a deformed mesh, which accounts for the material deposited in the cathode and the material removed from the anode.

To select a suitable mesh in terms of stability of calculated values and simulation time, a mesh analysis was performed, using a free tetrahedral mesh with the following features:

- The number of elements over the cathode and anode was prescribed.
- A maximum element size was imposed in the whole domain.
- A refinement of element size was imposed in the remaining boundaries and corners (rod, jar walls and liquid surface).
- A boundary layer option is used in the moving and fixed walls, except the liquid surface.

Gradually more refined meshes were tested and the velocity magnitude at selected locations (Fig. 4) were compared.

The theoretical area of cathode assuming a perfectly straight profile is 0.1868 dm^2. As can be seen in Fig. 5, the vertical side of the experimental cathode is slightly curved, and this initial shape was considered in the geometry of the system (see following sections). Therefore, due to that curved profile, the actual active area is slightly higher (3–4%).

The fluid flow was solved using a segregated PARDISO solver, using 0.001 tolerance and maximum 300 iterations. The different turbulence models consider different groups of segregated values. For ternary current distribution, an initial solution for primary current distribution was obtained (MUMPS solver, 0.001 tolerance, and maximum 25 iterations). Next, the transient ternary current distribution was obtained using a BDF solver, with 1×10^{-8} seconds of initial step and maximum step of 2 s (at each time MUMPS solver is used, 0.001 tolerance, and maximum 5 iterations). In Nernst-Plank equation, all stabilization options were active in the solver, with values by default. Such options allow the model to achieve convergence relatively fast, even though the deposit could turn out to be slightly smaller at the edge. The model was solved in a Windows 10 PC Intel i7 7700 3.6 GHz, 16 GB RAM.

2.2. Model verification: electrodeposition of Zn

The RWE (8 mm inner diameter, 40 mm outer diameter), previously mentioned, was made from 0.7 mm thickness SAE 1010 steel strip and was cut with a high precision automatic laser-cutting machine. Then were mounted on a steel rod isolated with a Teflon cylinder, leaving an exposed area of 0.19 dm^2. A 70 mm internal diameter ring of pure zinc ingot was cast and used as anode.

Washer rotation speed (*w*) was varied between 400 and 1200 rpm throughout the tests. The average rotation speed (800 rpm) was selected considering that usually, the electrolyte in the industrial process has a counter current flow, with respect to the direction in which the strip advances, at a speed of 1 m/s while the average line speed is 0.67 m/s. Hence, tangential speed at the edge of the disk in rotation was adjusted

Table 2
Mesh analysis.

# Elements	Velocity magnitude (m/s), point:						CFD		Ternary current distribution	
	1	2	3	4	5	6	DOF	ST (s)*	DOF	ST (s)* *
5432	0.156	0.421	0.151	0.471	0.165	0.278	25928	30	37105	137
6284	0.170	0.425	0.162	0.450	0.168	0.288	31129	32	44531	141
15497	0.175	0.415	0.164	0.463	0.171	0.318	77203	45	111548	553
21967	0.177	0.412	0.166	0.447	0.173	0.295	108766	70	157470	676
25978	0.179	0.418	0.167	0.458	0.172	0.300	128317	82	185917	810
27022	0.181	0.417	0.167	0.449	0.174	0.301	133266	84	193105	1028
29722	0.182	0.415	0.168	0.447	0.174	0.301	146272	90	212021	1149
33076	0.184	0.417	0.169	0.450	0.174	0.300	162582	118	235743	1191

* * Simulation time (ST) including steady primary current distribution, and transient ternary current
* Starting the solver from a previous steady solution

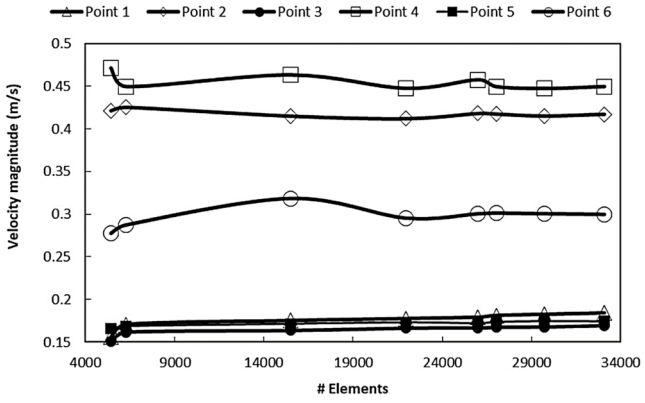

Fig. 6. Comparison of the meshes detailed in Table 2 in terms of velocity magnitude. Points locations are shown in Fig. 4.

to be equal to the sum of the electrolyte speed plus the advance speed of the steel strip: 1 m/s + 0.67 m/s = 1.67 m/s which gives a rotation speed of 800 rpm [9].

The electrolyte used was a 90 g/L zinc sulfate solution prepared diluting $ZnSO_4{\cdot}7\ H_2O$ (Biopack, 99.9%) with double distilled water. The pH was adjusted to 2 (20 °C), adding sulfuric acid (Anedra, 98%). The temperature of the solution was controlled using a Frigomix 1495 thermostatic bath and a double wall cell. Current density (i_C) was varied with a DC power supply (Full Energy HY3020 model). Electrodeposition time was set to have a theoretical average zinc thickness (AT) of 14.8 μm. The experimental conditions are shown in Table 1.

Samples 1–4 were weighted before and after electrodeposition of Zn and the AT was calculated using Eq. (6) and later, compared to the value given by the model:

$$AT \quad (\mu m) = \frac{(m_a - m_b)}{\rho_{Zn} A} \tag{6}$$

being m_b the cathode mass before the electrodeposition and m_a the cathode mass after the experiment; ρ_{Zn} is the density of Zn (7138 kg/m^3).

Coatings cross sections were embedded in an epoxy resin, ground using 80 to 2500 grade silicon paper and polished with 1 μm diamond paste. Scanning electron microscopy (SEM) was used to measure the thickness of Zn coatings (Quanta200 FEI microscope). The thickness values were compared to those calculated by the model to validate its accuracy and the spatial distribution of the Zn deposit.

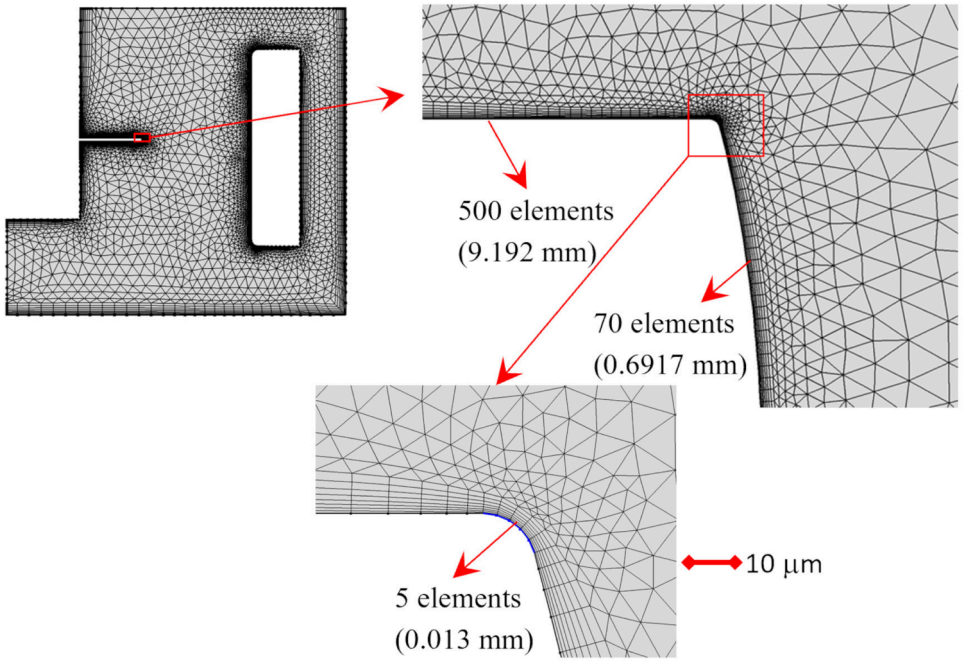

Fig. 7. Elements in the final mesh.

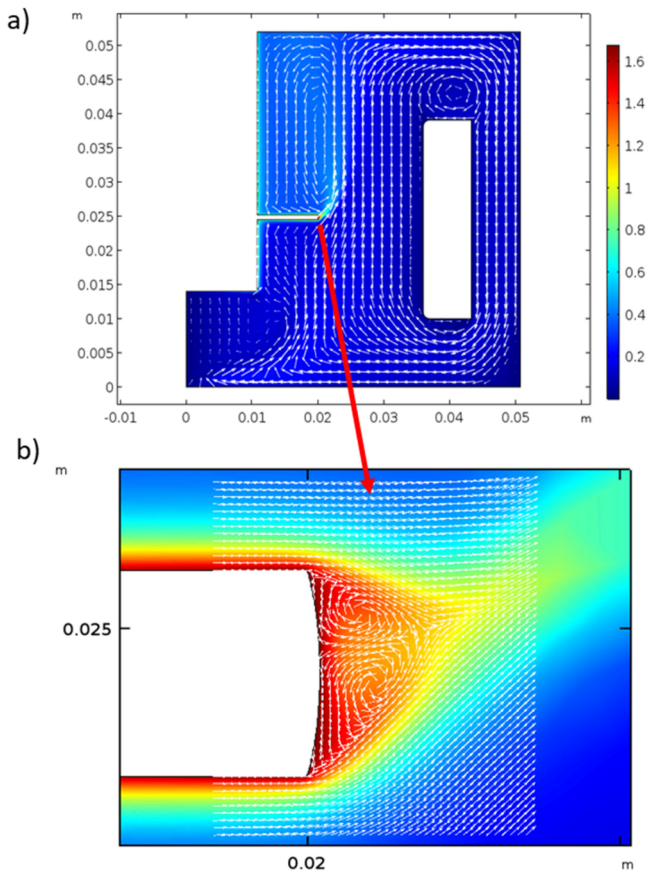

Fig. 8. a) Velocity magnitude in the electrolyte for sample 10, b) detail of velocity field around the cathode.

3. Results and discussion

3.1. Simulation results

3.1.1. Mesh analysis

Table 2 shows the details of the mesh analysis, for sample 5; for it the highest current density was used, which can cause convergence issues in the numerical method. A coarse mesh of 5432 elements to an extremely fine mesh of 33076 elements. "Fine" refinement with a maximum element size of 0.0018 m was used in the whole domain, and "Finer" refinement was imposed in the remaining boundaries and corners, and a "boundary layer" option was used in the moving and fixed walls (8 layers, 1.2 increment factor). Based on the velocity results showed in Table 2 and Fig. 6, the sixth mesh of Table 2 (27022 elements between triangles and rectangles), was selected to complete the simulation. This mesh had 410 elements on each horizontal side of the cathode, 50 elements on the vertical side, and 5 elements on the fillet corner (Fig. 7). In the anode, 130 elements were used.

3.1.2. Simulated results

Fig. 8 shows a surface plot of the velocity magnitude in the electrolyte and an arrow plot of the velocity field is included. A large vortex can be seen near the extreme of the cathode (highlighted in the enlarged image); also swirls above and beyond the cathode surface can be identified.

Fig. 9 shows total mass flux (mol/(m^2 s) (sample 10, t = 60 s) and it is worth noting the magnitude of each mass transfer mechanism: convection, 10^3; diffusion and electrophoretic migration, 10^{-2}. According to these relative values, diffusion and migration could be neglected in the solution of more complex systems (larger scale, finer meshes, irregular complex geometries), to decrease calculation times.

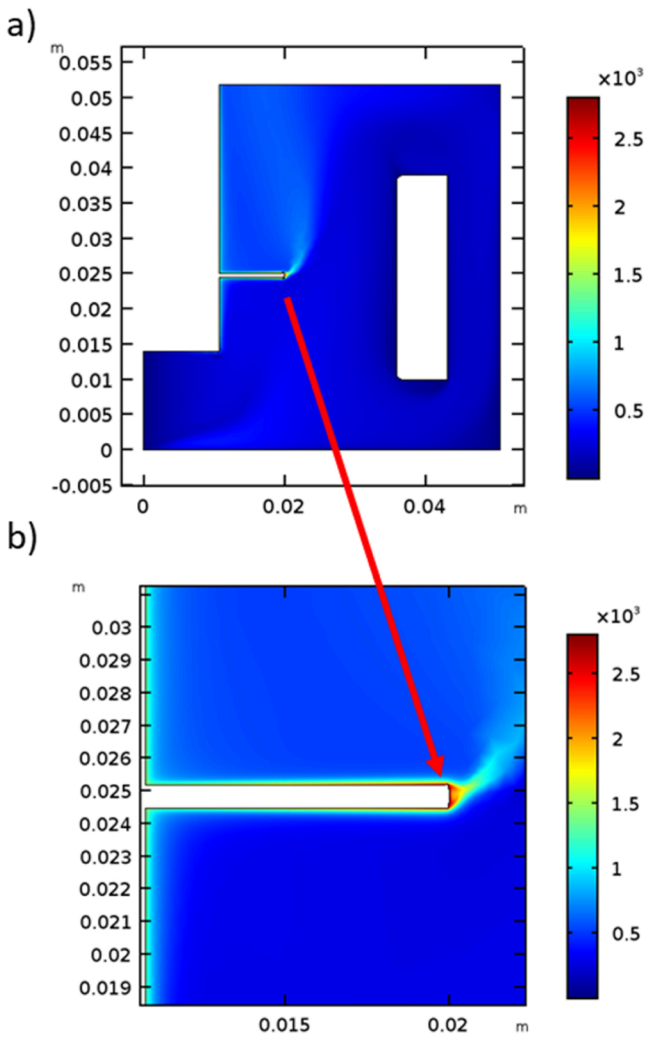

Fig. 9. a) Total mass flux [mol/(m^2 *s)], for sample 10, t = 60 s, b) detail around the cathode.

Fig. 10 shows the local current density (in absolute values) and the local thickness of deposited material along the cathode arc length. Maximum values of current density occur in the corners, due to the primary current distribution, i. e. electrolyte resistivity and geometric aspects. The variation of local deposit thickness is completely analogous: higher thicknesses are obtained where the current density is higher.

3.2. Model validation

The described model was validated with experimental results of zinc electrodeposition on the RWE. According to the experimental set-up and Faraday's law of electrolysis, a Zn deposit with an AT of 14.8 μm should be obtained. The results of the AT determined by gravimetry (quadruplicate, Eq. (6)) gave 14.8 ± 0.2 μm and were comparable to the theoretical one. Also, the AT calculated from the total charge estimated by integration of current density along the surface of the cathode, for these samples, differed less than 1% from the weight-determined value. Both results allowed us to confirm the appropriateness of the chosen parameters, which were later refined and improved.

The model predicts an AT between 14.5 and 14.6 μm (Table 3) values in good agreement with the theoretical value. From the simulated results, the minimum (7.4–7.8 μm) and maximum (57.8–67.5 μm) local deposit thicknesses were obtained.

Samples 5–10 were cut, embedded in epoxy resin and their cross sections were observed by SEM. The thickness of the Zn coating was

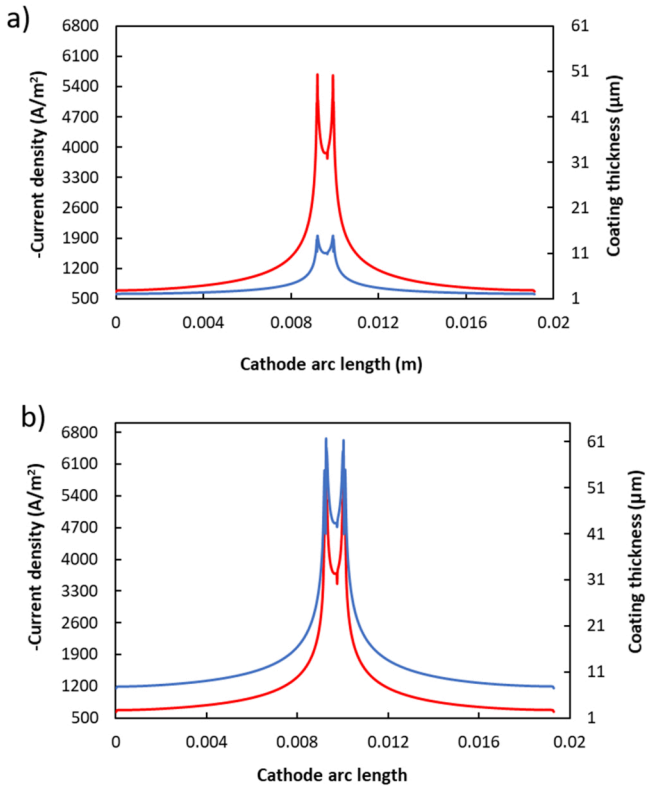

Fig. 10. Cathode current density (red line, absolute values) and coating thickness (blue line) vs. arc length for sample 10, a) 60 s and b) 240 s.

Table 3
Simulated AT values (µm), standard deviation SD, minimum and maximum thickness of Zn coating.

Sample	AT (µm)	SD (µm)	Minimum (µm)	Maximum (µm)
5	14.5	6.7	7.6	64.8
6	14.5	6.8	7.5	64.3
7	14.6	6.5	7.8	57.8
8	14.5	6.9	7.4	67.5
9	14.6	6.6	7.4	61.9
10	14.5	6.7	7.5	64.0

measured along the arc and compared with the values predicted by the model. The results for samples 7 and 10 are presented in Fig. 11. The maximum thickness is located at the edges of the electrode, where the current density is higher. This is consistent with the coating thickness distribution predicted by the model, as previously discussed (Fig. 10).

A SEM image of the cross section of sample 10 (200X) is presented overlaid with the model results (Fig. 12). The initial shape of the steel cathode is drawn in green dots while the simulated deposit shape is represented in red dots. The predicted geometries are in good agreement with the experimental ones.

It is worth noting that deviations between measured and predicted values become larger at the corners of the cathode. Even though the model predicts the general profile of deposited Zn, at these points higher thicknesses are observed experimentally. The corner may be acting as a protuberance growing faster than the rest of the coating [5,23]. According to dendritic growth theory, a spherical diffusion geometry develops at these points and modified kinetic equations should be used to describe the process. Despite this drawback, the model accurately predicts the global behavior of the RWE and the electroplating cell. Hence, it was as a valuable experimental system to study the effect of process variables on the current distribution.

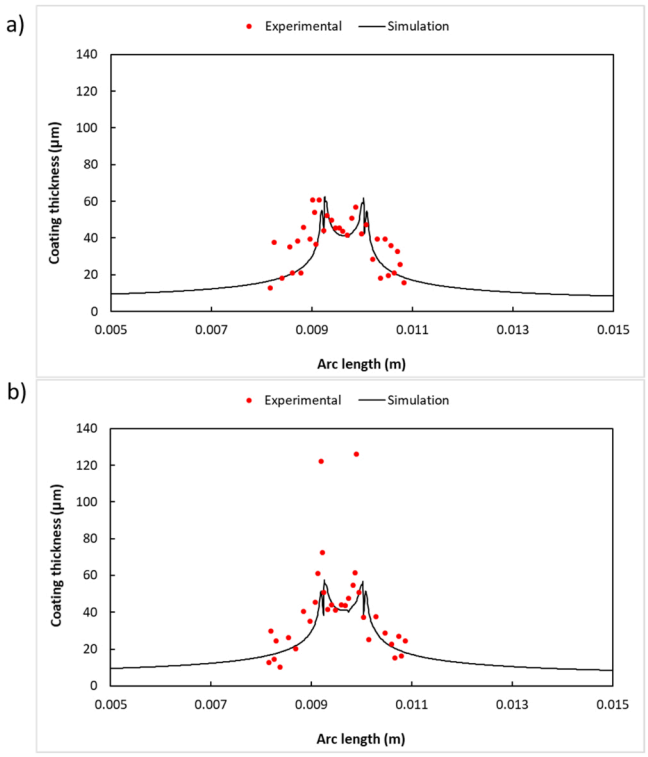

Fig. 11. Measured vs. simulated coating thickness a) sample 7, b) sample 10.

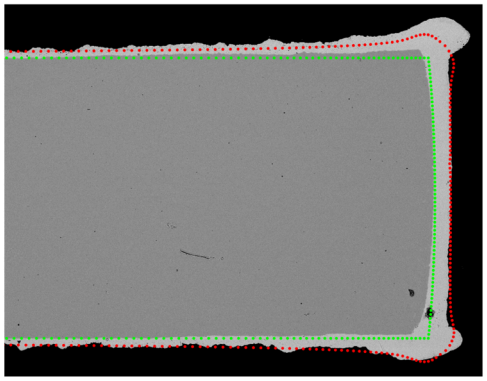

Fig. 12. Cross section of sample 10 observed by SEM (200X). Simulated results: initial geometry (green dots), final geometry including deposit (red dots).

4. Conclusions

A mathematical model of zinc electrodeposition on moving cathodes was developed. This model is a promising tool to study complex electrochemical systems commonly used in electroplating laboratories and related industrial processes where the fluid dynamic, mass flow and electrochemistry are strongly linked.

Using this model, it is possible to evaluate the effect of several operating variables like temperature, voltage difference, average density, rotating speed, on the thickness distribution of the metal deposit. This is valuable information in processes where a uniform thickness is required as in the case of zinc electrodeposition.

The validation of the model with the RWE gives a solid background to this electrochemical setup and expands its application to several new alternatives to study real systems, e.g. determining changes in kinetics parameters after addition of additives and later feeding this information into the mathematical model might help to identify and select the right levelling agents, to study edge masks design, to change the depositing

metal or even study alloy deposition.

Finally, the model was validated, and it has been proven that the set of equations and boundary conditions properly describe the phenomena involved.

Declaration of Competing Interest

The authors declare that they have no known competing financial interests or personal relationships that could have appeared to influence the work reported in this paper.

Data Availability

Data will be made available on request.

Acknowledgements

Financial support to conduct this study was provided by Comisión de Investigaciones Científicas de la Provincia de Buenos Aires (CICPBA), Consejo Nacional de Investigaciones Científicas y T é cnicas (CONICET), Agencia Nacional de Promoción Científica y Tecnológica (PICT 2018–3499) and Universidad Nacional de La Plata (UNLP). The authors wish to thank these institutions for the funds allocated to this investigation.

References

[1] R. Winand, Electrodeposition of zinc and zinc alloys, Mod. Electroplat. (2010) 423–460.
[2] J.H. Lindsay, T.J. O'Keefe, Electrogalvanizing, in: Modern Aspects of Electrochemistry, Springer, 1994, pp. 165–228.
[3] A.R. Despić, K.I. Popov, Transport-controlled deposition and dissolution of metals. in: Modern Aspects of Electrochemistry No. 7, Springer,, 1972, pp. 199–313.
[4] K.I. Popov, M.G. Pavlović, Electrodeposition of metal powders with controlled particle grain size and morphology, in: Modern Aspects of Electrochemistry, Springer, 1993, pp. 299–391.
[5] K.I. Popov, N.V. Krstajic, M.I. Cekerevac, The mechanism of formation of coarse and disperse electrodeposits, Mod. Asp. Electrochem. 30 (1996) 261–312.
[6] K. Popov, B. Grgur, S.S. Djokić, Fundamental Aspects of Electrometallurgy, Springer, 2007.
[7] G. Wranglén, Dendrites and growth layers in the electrocrystallization of metals, Electrochim Acta 2 (1960) 130–143.
[8] L.N. Bengoa, S. Bruno, H.A. Lazzarino, P.R. Seré, W.A. Egli, Study of dendritic growth of zinc crystals on the edges of steel sheet, J. Appl. Electrochem 44 (2014) 1261–1269, https://doi.org/10.1007/s10800-014-0722-y.
[9] L.N. Bengoa, S. Bruno, H.A. Lazzarino, P.R. Seré, W.A. Egli, Dendritic zinc growth on the edges of flat steel strip during electro galvanizing, Procedia Mater. Sci. 8 (2015) 1174–1183, https://doi.org/10.1016/j.mspro.2015.04.183.
[10] L.N. Bengoa, P.R. Seré, M.S. Conconi, W.A. Egli, Morphology and texture of zinc deposits formed at the edge of a rotating washer electrode, J. Mater. Eng. Perform. 25 (2016) 2936–2942, https://doi.org/10.1007/s11665-016-2163-8.
[11] L.N. Bengoa, P. Pary, P.R. Seré, M.S. Conconi, W.A. Egli, Dendritic zinc growth in acid electrolyte: effect of the pH, J. Mater. Eng. Perform. 27 (2018) 1103–1108, https://doi.org/10.1007/s11665-018-3139-7.
[12] A. Vagaská, Mathematical-statistical nonlinear model of zincing process and strategy for determining the optimal process conditions, Mathematics 1 (2023) 771, https://doi.org/10.3390/math11030771.
[13] D. Solovjev, I. Solovjeva, V. Konkina, Mathematical modelling and optimization of the electroplating process with a rotating cathode to reduce the non-uniformity of the coating thickness, MATEC Web Conf. 298 (2019) 00014, https://doi.org/10.1051/matecconf/201929800014.
[14] M. Robison, M.L. Free, Modeling and experimental validation of electroplating deposit distributions from copper sulfate solutions, ECS Trans. 61 (2014) 27–36, https://doi.org/10.1149/06121.0027ecst.
[15] J.M. Werner, W. Zeng, M.L. Free, Z. Zhang, J. Cho, Editors' choice—modeling and validation of local electrowinning electrode current density using two phase flow and nernst–planck equations, J. Electrochem Soc. 165 (2018) E190–E207, https://doi.org/10.1149/2.0581805jes.
[16] A. Mahapatro, S.K. Suggu, Modeling and simulation of electrodeposition: electrolyte current density and conductivity on electroplating thickness, Adv. Mater. Sci. 3 (2) (2018) 1–9, https://doi.org/10.15761/AMS.1000143.
[17] A.A. da C. Bastos, Simulación 3D de la distribución espacial de especies químicas asociadas a la corrosión del par Zn-Fe, Universidad de Málaga, 2021.
[18] A.J. Mohammed, Zinc plating from alkaline non-cyanide bath, Missouri UNiversity Of Science and Technology, 2022.
[19] E.P. Rivero, P. Granados, F.F. Rivera, M. Cruz, I. González, Mass transfer modeling and simulation at a rotating cylinder electrode (RCE) reactor under turbulent flow for copper recovery, Chem. Eng. Sci. 65 (2010) 3042–3049, https://doi.org/10.1016/j.ces.2010.01.030.
[20] F.J. Almazán-Ruiz, F.V. Caballero, M.R. Cruz-Díaz, E.P. Rivero, I. González, Scale-up of rotating cylinder electrode electrochemical reactor for Cu(II) recovery: experimental and simulation study in turbulence regimen, Electro Acta 77 (2012) 262–271, https://doi.org/10.1016/j.electacta.2012.06.003.
[21] E. Guerra, M. Bestetti, Physicochemical properties of ZnSO4-H2SO 4-H2O electrolytes of relevance to zinc electrowinning, J. Chem. Eng. Data 51 (2006) 1491–1497, https://doi.org/10.1021/je0600911.
[22] E. Yeager, J.O. Bockris, B. Conway, S. Sarangapani, Volume 6, Electrodics: transport, in: Comprehensive Treatise of Electrochetnistry, Springer, 1983.
[23] K.I. Popov, N.D. Nikolić, General theory of disperse metal electrodeposits formation, in: Electrochemical Production of Metal Powders, Springer, 2012, pp. 1–62.